Ionic selectivity and filtration from fragmented dehydration in multilayer graphene nanopores – Supplementary Information

Subin Sahu[1,2,3] and Michael Zwolak[1,*]

[1] *Center for Nanoscale Science and Technology, National Institute of Standards and Technology, Gaithersburg, MD 20899*

[2] *Maryland Nanocenter, University of Maryland, College Park, MD 20742*

[3] *Department of Physics, Oregon State University, Corvallis, OR 97331*

CONTENTS

* mpz@nist.gov

I. METHODS

A. All-atom MD simulations

We use multilayer graphene with AB stacking with a C-C bond length of ≈ 0.14 nm and inter-layer distance of ≈ 0.335 nm. We open a pore of nominal radius r_n at the center of each membrane by removing carbon atoms whose coordinates satisfy the condition $(x - x_c)^2 + (y - y_c)^2 < r_n^2$, where (x_c, y_c) is the center of mass in each graphene membrane. However, the pore radius, r_p, is measured from the inner edge of carbon atoms (taken as their van der Waals radius) around the pore. The graphene membrane has a square cross-section of 7.2 nm by 7.2 nm, which we immerse in an aqueous KCl solution of concentration 1 mol/L that extends 5 nm on both sides of the membrane.

We perform all-atom molecular dynamics (MD) simulations using NAMD2 [1] with a time step of 2 fs and employ periodic boundary condition in all directions. The water model in our simulation is rigid TIP3P [2] from the CHARMM27 force field (previously, we used flexible TIP3P [3, 4], which gives similar results but the rigid model allows for more efficient simulations). Non-bonded interactions (van der Waals and electrostatic) have a cutoff of 1.2 nm, but we perform a full electrostatics calculation every 8 fs using particle-mesh Ewald (PME) method [5]. We prepare the system using VMD [6] and then equilibrate the system using NAMD2. The equilibration steps are (1) minimizing the energy of the system for 4000 steps, (2) heating it to 295 K in another 8 ps, (3) a 1 ns NPT (constant number of particles, pressure and temperature) equilibration using the Nose-Hoover Langevin piston method [7] to raise the pressure to 101325 Pa (i.e., 1 atm), and (4) a 3 ns of NVT (constant number of particles, volume and temperature) equilibration.

We use real-time, all-atom molecular dynamics simulations to calculate the ionic current through the equilibrated system by applying an electric field perpendicular to the plane of the membrane. We set the Langevin damping rate to 0.2 ps^{-1} for carbon and water (via its oxygen atoms) during these runs. We freeze the carbon atoms at the outer edge of the graphene membrane, but the rest of the carbon atoms in the graphene membrane are only confined by C-C bonds. We averaged the current for a total time of 50 ns to 150 ns depending on the pore size and number of layers.

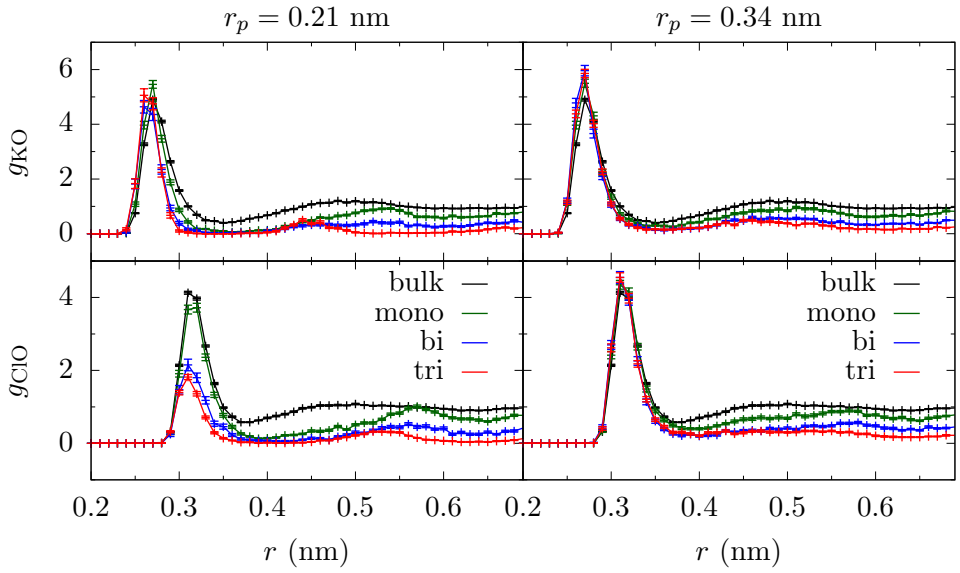

FIG. S-1. Radial distribution functions g_{KO} and g_{ClO} with K^+ and Cl^- ions in bulk and inside the mono-, bi-, and tri-layer graphene pores with radius $r_p = 0.21$ nm and $r_p = 0.34$ nm. The bulk ion concentration is maintained at 1 mol/L in each calculation. There is significant dehydration in both the first and second hydration layers in the $r_p = 0.21$ nm pore, whereas in the $r_p = 0.34$ nm pore dehydration is significant only in the second hydration layer. The error bars are ± 1 block standard error (BSE).

B. Solvation Shells

To calculate the solvation shells for each ion, we fix the ion in the center of a pore and run equilibrium NVT simulations. Fig. S-1 shows the radial distribution functions of oxygen atoms with respect to the ion (K^+ or Cl^-) fixed in the bulk and in the center of the pore in mono-, bi-, and tri-layer graphene. Fig. S-2 shows the solvation shell around K^+ and Cl^- ions fixed at the center of 0.21 nm pore on mono-, bi-, and tri-layer graphene. A similar plot for 0.34 nm pore is shown in Fig. 1(b) of the main text. These plots show that in monolayer graphene, the ion at the center of the pore can maintain most of its first hydration shell. However, in bi- and tri-layer graphene there is a greater loss of water from first hydration layer. The dehydration is even stronger in the second hydration layer, losing about 50 %, 80 %, and 90 % of water molecules in mono-, bi-, and tri-layer graphene, respectively. The water molecules around the ion in the pore are spatially localized, thus giving fragmented solvation shells. We note that in Fig. 2(b) of the main text, we calculate the fractional

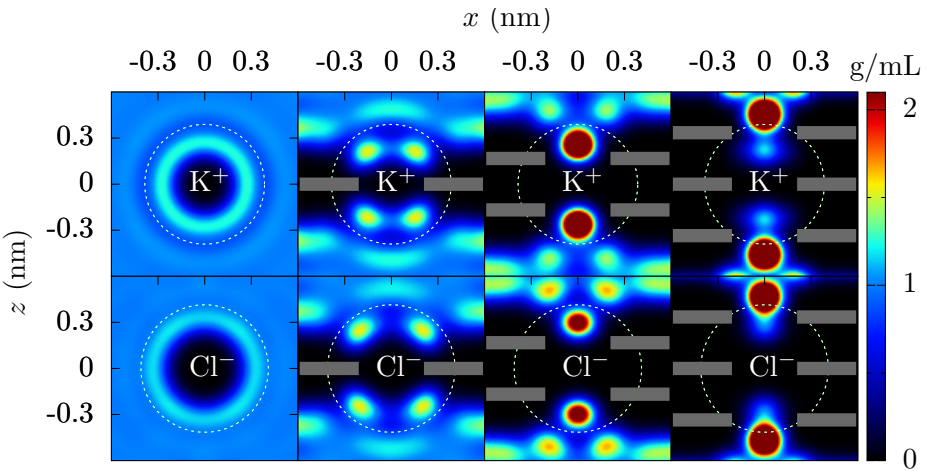

FIG. S-2. Water density (within the $y = 0$ plane) quantified by its oxygen location around K^+ and Cl^- ions in bulk and mono-, bi-, and tri-layer graphene (shown as gray bars) pores with radius $r_p = 0.21$ nm. The white dotted circles demarcate the first and the second hydration layers. The bi- and tri-layer graphene significantly excludes both the first and second hydration layers. For monolayer graphene, however, most of the hydration layers are still present due to the atomic thickness of the membrane (see Table S-2). However, the water molecules are more localized than in bulk.

dehydration with the ion within a distance 0.1 nm of its free energy maximum position along z-axis, as this is the most relevant location in determining ion transport.

C. Free Energy Calculations

We calculate the free energy profile of an ion crossing the pore by using the adaptive biasing force (ABF) method [8, 9] as implemented in NAMD2. We compute the free energy barrier within a cylinder of radius r_p and height of 3 nm centered at the origin. Fig. S-3 shows the free-energy profile for both K^+ and Cl^- ions and the difference in the free energies of these two ions along the z-axis. The free energy barrier for each ion increases as we decrease the pore radius or increase the number of graphene layers. Also, the difference in the free energy barriers of K^+ and Cl^- increases for decreasing pore radius and increasing number of graphene layers. The free energy barriers appear due to dehydration of ions in the pore (see Fig. S-4). As pore radius decreases and the number of graphene layer increases, the fractional dehydration in the solvation shell of ion increases, as shown in Fig. S-4 and

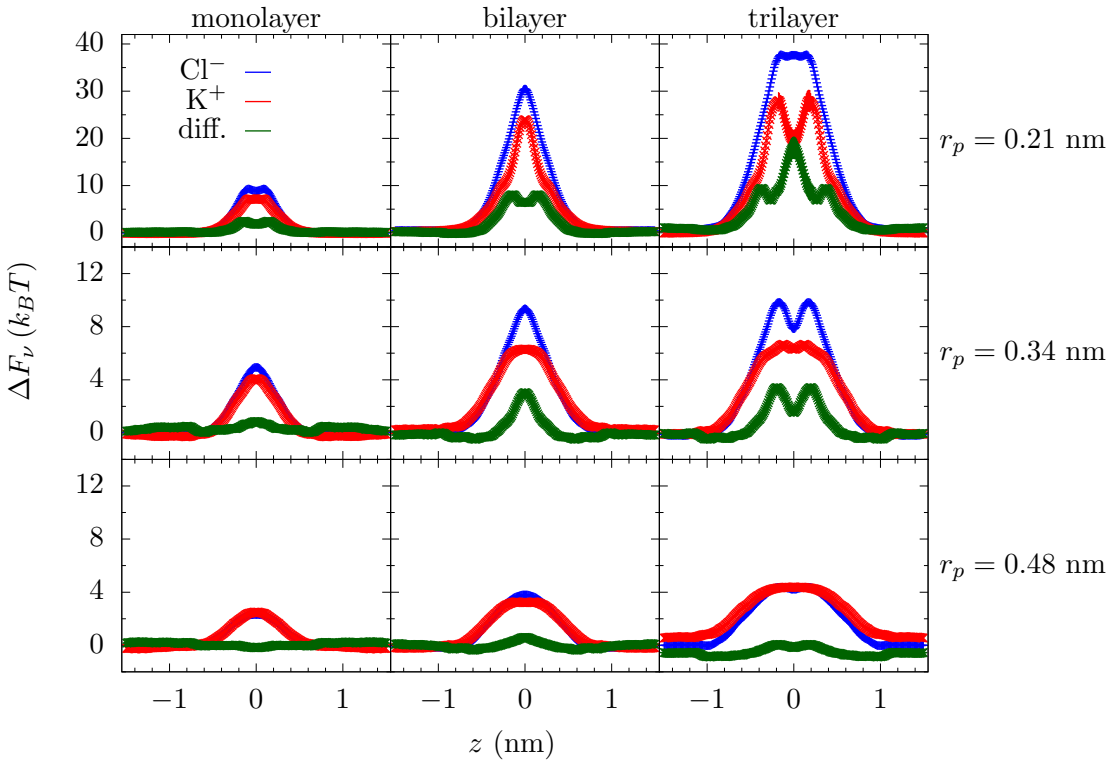

FIG. S-3. Free energy barrier for K^+ (red line) ion, Cl^- (blue line) ion, and their difference (green line) to translocate through the pore versus the z-location for radii 0.21 nm, 0.34 nm, and 0.48 nm pores in mono-, bi-, and tri-layer graphene. The free energy barriers, as well as their difference, increase with decreasing pore radius and with increasing number of graphene layers, thus making the pore more selective. Error bars are ±1 standard error from five parallel simulations.

Fig. 2(b) of the main text.

II. "QUANTIZED" IONIC CURRENT

Since the ion current density relates to the free energy barrier as $J_\nu = J_{\nu 0} e^{-\Delta F_\nu / k_B T}$ and the energy barrier is related to the number of waters lost from the solvation shell, the ionic current is expected to have a step-like feature with respect to the pore size, as this determines the extent of dehydration. We see indications of such step-like features in current density, as shown in Fig. S-5(a). However, the pore sizes themselves are "discretized" at this length scale (and not perfectly circular), it is hard to determine if these features are sharp. As we mention in the main text, irregularly shaped nanopores may allow one to examine

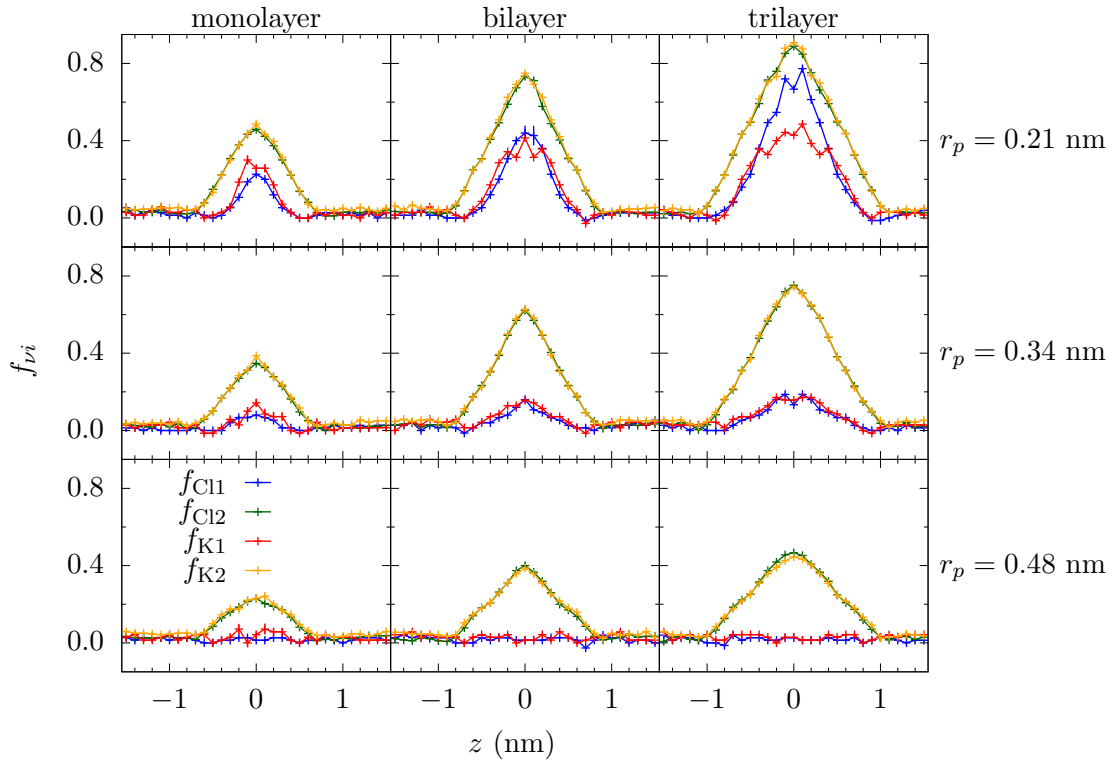

FIG. S-4. Fractional dehydration in the first and the second hydration layers for K^+ and Cl^- ions translocating through pores of radius 0.21 nm, 0.34 nm, and 0.48 nm in mono-, bi-, and tri-layer graphene. These results come from the same simulation as used to compute the free energy barrier. Just like the free energy barrier, the dehydration increases with the decrease in the pore radius and with the increase in the number of graphene layers. Fractional dehydration is always smaller in the first hydration layer compare to the second hydration layer. However, due to the larger energy of the first hydration layer, it still has a large contribution to the free energy barrier. Error bars are ±1 standard error from five parallel simulations.

intermediate pore sizes and determine if these step features are indeed sharp. We leave this for a future study, although it is clear from Fig. S-5(a) that there is a change in current density when the second (for bi- and tri-layer graphene) and first hydration layers (for all cases) are encroached upon.

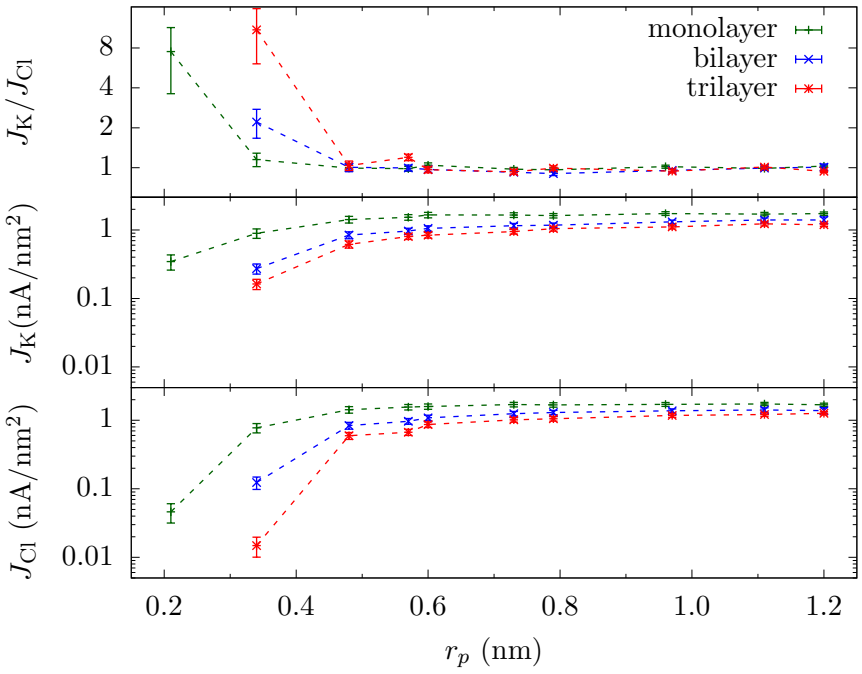

FIG. S-5. Current densities in the pore, $J_K = I_K/\pi r_p^2$ and $J_{Cl} = I_{Cl}/\pi r_p^2$, and their ratio versus r_p for mono-, bi-, and tri-layer graphene membranes. There is no selectivity ($I_K/I_{Cl} \approx 1$) until both the length and radius of the channel significantly encroach on the hydration layers. This occurs for a larger radius for bi- and tri-layer graphene as both the first and second hydration layer are more significantly diminished due to the larger pore length. Moreover, J is fairly constant for r_p greater than the second hydration layer radius (≈ 0.6 nm) and starts to drop as pore size decreases further. The drop is much sharper below the first hydration layer (≈ 0.3 nm) to the extent that we find no current for bi- and tri-layer graphene within the time of our simulations. The error bars are $\pm$ 1 BSE.

III. DATA

	monolayer									
r_p (nm)	0.21	0.34	0.48	0.57	0.6	0.73	0.79	0.96	1.11	1.2
I_{K} (nA)	0.048	0.33	1.03	1.56	1.87	2.77	3.18	5.03	6.6	7.8
I_{Cl} (nA)	0.006	0.28	1.03	1.59	1.79	2.84	3.29	4.94	6.7	7.7
$I_{\mathrm{K}}/I_{\mathrm{Cl}}$	8	1.2	1.0	1.0	1.0	1.0	1.0	1.0	1.0	1.0
	bilayer									
r_p (nm)	0.16	0.34	0.48	0.57	0.6	0.73	0.79	0.97	1.11	1.2
I_{K} (nA)	0	0.10	0.61	0.98	1.19	1.93	2.30	3.88	5.4	6.3
I_{Cl} (nA)	0	0.04	0.60	0.99	1.23	2.09	2.55	4.06	5.5	6.3
$I_{\mathrm{K}}/I_{\mathrm{Cl}}$	-	2.2	1.0	1.0	1.0	1.0	1.0	1.0	1.0	1.0
	trilayer									
r_p (nm)	0.14	0.34	0.48	0.57	0.6	0.73	0.79	0.97	1.11	1.2
I_{K} (nA)	0	0.059	0.45	0.82	0.95	1.59	2.05	3.28	4.8	5.4
I_{Cl} (nA)	0	0.005	0.43	0.68	0.98	1.70	2.06	3.48	4.7	5.7
$I_{\mathrm{K}}/I_{\mathrm{Cl}}$	-	11	1.0	1.2	1.0	1.0	1.0	1.0	1.0	1.0

TABLE S-1. K^+ and Cl^- currents and their ratio in pores of various radii in mono-, bi- and tri-layer graphene. We measure the currents by counting the ions that cross through the pore. There were no ion crossing events for the smallest pore in bi- and tri-layer graphene. The error in current is ≈ 20 % for $r_p = 0.21$ nm and ≈ 10 % for $r_p = 0.34$ nm and ≈ 2 % for larger pores.. The error in selectivity is shown in Fig. S-5.

	K^+				Cl^-			
	$r_p = 0.21$ nm		$r_p = 0.34$ nm		$r_p = 0.21$ nm		$r_p = 0.34$ nm	
	n_1	n_2	n_1	n_2	n_1	n_2	n_1	n_2
monolayer	4.7 (3.7)	13.1 (13.1)	7.6 (6.4)	15.9 (15.6)	5.1 (3.8)	15.4 (16.6)	7.7 (6.6)	17.8 (15.8)
bilayer	3.0 (2.8)	5.1 (7.0)	7.3 (6.4)	9.7 (7.9)	2.4 (2.4)	6.5 (7.0)	7.4 (6.6)	11.1 (7.9)
trilayer	4.0 (2.8)	2.1 (2.0)	7.3 (6.4)	8.2 (6.4)	4.0 (2.4)	2.2 (1.7)	7.7 (6.6)	8.8 (5.0)
bulk	6.8	23.0	6.8	23.0	7.4	26.3	7.4	26.3

TABLE S-2. The average number of water molecules, $\langle n \rangle$, in the first and second hydration layer for K^+ and Cl^- ions fixed at the center of the two smallest pores and in bulk. The error in $\langle n \rangle$ is $\approx \pm 0.01$ in each case. The estimated water loss considering only the geometric confinement is shown in parentheses. For the geometric estimate, mono-, bi-, and tri graphene is approximated as a cylindrical hole of thickness 0.3, 0.6 and 0.9 nm, respectively.

	K^+		Cl^-	
	$r_p = 0.21$ nm	$r_p = 0.34$ nm	$r_p = 0.21$ nm	$r_p = 0.34$ nm
monolayer	2.0	1.3	-1.6	-1.5
bilayer	2.2	1.4	-1.9	-1.5
trilayer	2.1	1.3	-1.8	-1.4
bulk	1.4	1.4	-1.4	-1.4

TABLE S-3. Average dipole orientation (in Debye) along the radial direction $\langle p_r \rangle$ in the first hydration layer of K^+ and Cl^- ions fixed in the center of the two smallest pores and in bulk. The total dipole moment of individual water molecule in our model is 2.35 D, thus water molecule in the $r_p = 0.21$ nm pore in bi- and tri-layer graphene are almost perfectly oriented along radial direction. The error in $\langle p_r \rangle$ is $\approx \pm 0.01$ in each case. Overall ion concentration is maintained at 1 mol/L in each case. When more water is excluded, especially from the first hydration layer, the remaining water more strongly orients its dipole to energetically compensate for the water loss.

[1] J. C. Phillips, R. Braun, W. Wang, J. Gumbart, E. Tajkhorshid, E. Villa, C. Chipot, R. D. Skeel, L. Kale, and K. Schulten, J. Comput. Chem. **26**, 1781 (2005).

[2] W. L. Jorgensen, J. Chandrasekhar, J. D. Madura, R. W. Impey, and M. L. Klein, J. Chem. Phys. **79**, 926 (1983).

[3] S. Sahu, M. Di Ventra, and M. Zwolak, arXiv:1605.03134 (2016).

[4] S. Sahu, M. Di Ventra, and M. Zwolak, Nano Lett. (2017), 10.1021/acs.nanolett.7b01399.

[5] T. Darden, D. York, and L. Pedersen, J. Chem. Phys. **98**, 10089 (1993).

[6] W. Humphrey, A. Dalke, and K. Schulten, J. Mol. Graphics **14**, 33 (1996).

[7] G. J. Martyna, D. J. Tobias, and M. L. Klein, J. Chem. Phys. **101**, 4177 (1994).

[8] E. Darve, D. Rodríguez-Gómez, and A. Pohorille, J. Chem. Phys. **128**, 144120 (2008).

[9] J. Hénin and C. Chipot, J. Chem. Phys. **121**, 2904 (2004).